








## A multi-model assessment of the Global Warming Potential of hydrogen

Maria Sand <sup>1</sup>✉, Ragnhild Bieltvedt Skeie <sup>1</sup>, Marit Sandstad <sup>1</sup>, Srinath Krishnan<sup>1</sup>, Gunnar Myhre <sup>1</sup>, Hannah Bryant<sup>2</sup>, Richard Derwent <sup>3</sup>, Didier Hauglustaine<sup>4</sup>, Fabien Paulot <sup>5</sup>, Michael Prather <sup>6</sup> & David Stevenson<sup>2</sup>

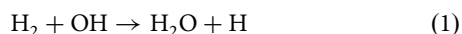
With increasing global interest in molecular hydrogen to replace fossil fuels, more attention is being paid to potential leakages of hydrogen into the atmosphere and its environmental consequences. Hydrogen is not directly a greenhouse gas, but its chemical reactions change the abundances of the greenhouse gases methane, ozone, and stratospheric water vapor, as well as aerosols. Here, we use a model ensemble of five global atmospheric chemistry models to estimate the 100-year time-horizon Global Warming Potential (GWP100) of hydrogen. We estimate a hydrogen GWP100 of  $11.6 \pm 2.8$  (one standard deviation). The uncertainty range covers soil uptake, photochemical production of hydrogen, the lifetimes of hydrogen and methane, and the hydroxyl radical feedback on methane and hydrogen. The hydrogen-induced changes are robust across the different models. It will be important to keep hydrogen leakages at a minimum to accomplish the benefits of switching to a hydrogen economy.

<sup>1</sup>CICERO Center for International Climate Research, Oslo, Norway. <sup>2</sup>School of Geosciences, University of Edinburgh, Edinburgh, UK. <sup>3</sup>rdscientific, Newbury, UK. <sup>4</sup>Laboratoire des Sciences du Climat et de l'Environnement (LSCE), CEA-CNRS-UVSQ, Université Paris-Saclay, Gif-sur-Yvette, France. <sup>5</sup>Geophysical Fluid Dynamics Laboratory, National Oceanic and Atmospheric Administration, Princeton, NJ, USA. <sup>6</sup>Earth System Science Department, University of California Irvine, Irvine, CA, USA. ✉email: [maria.sand@cicero.oslo.no](mailto:maria.sand@cicero.oslo.no)

When hydrogen ( $H_2$ ) is produced, transported, stored, and used, some fraction of the gas will leak to the atmosphere. In the existing value chain, there is very little data on the magnitude of these leakages and how this will evolve in a future growing hydrogen economy. Present-day hydrogen average abundances (mole fraction) are about 530 ppbv as reconstructed by firn air-derived estimates and atmospheric measurements<sup>1,2</sup>. Sources of hydrogen include biomass burning, fossil fuel combustion, biological nitrogen fixation, atmospheric photo-oxidation of methane and volatile organic compounds (VOCs) in the atmosphere, and possibly geological sources<sup>3</sup>. Hydrogen is removed from the atmosphere by biological uptake in soils and atmospheric oxidation by the hydroxyl radical (OH). The largest term, and the largest uncertainty term in the atmospheric hydrogen budget is the soil uptake, which in most studies accounts for 65–85% of the total hydrogen sink<sup>4–6</sup>. The atmospheric lifetime of hydrogen, defined as the total atmospheric burden divided by the total sinks, is about 2 years<sup>4</sup>.

Any Earth-system perturbation that impacts tropospheric chemistry creates a complex chain of events that alter radiatively active atmospheric species, such as methane, ozone, and aerosols, and hence perturbs Earth's radiative budget. Hydrogen is involved in atmospheric chemical reactions that affect the lifetime and abundances of other gases that have an impact on the climate<sup>7</sup> and is thus such an indirect greenhouse gas.

Four main climate impacts are associated with increased hydrogen levels: (1) a longer methane ( $CH_4$ ) lifetime and hence increased methane abundances, (2) an enhanced production of tropospheric ozone ( $O_3$ ) and changes in stratospheric  $O_3$ , (3) an increased stratospheric water vapor ( $H_2O$ ) production, and (4) changes in the production of certain aerosols. The most important reaction driving these impacts is the destruction of hydrogen by OH:



OH is the most important and powerful oxidant in the atmosphere<sup>8,9</sup>. Oxidation by OH is the major sink of hydrogen, methane, and other compounds in the atmosphere. The levels of OH in the atmosphere depend on other gases, most notably methane, nitrogen oxides (NO<sub>x</sub>), carbon monoxide (CO), and VOCs. All these processes are highly coupled and lead to chemical feedback processes<sup>10</sup>. Oxidation of methane and VOCs by OH also provides an important atmospheric source of hydrogen. Similarly, the change in chemistry caused by both the uptake of OH and production of H in reaction (1) can lead to changes in ozone. In the troposphere the production of water vapor is negligible compared to the natural water cycle<sup>11</sup>, but in the stratosphere, this reaction can affect the water vapor levels. Finally, changes in OH, ozone, and other oxidants may also affect the formation of particles, especially sulfate, secondary organic aerosols, and nitrate, and alter their size distributions<sup>12</sup>.

Global Warming Potentials (GWPs) allow comparisons of the global warming impacts of different gases, and hence hydrogen against other technologies. GWP is a useful metric, facilitating, for example, comparison of different implementations of a future hydrogen economy with other technologies that attempt to mitigate climate change<sup>13</sup>. A review on available literature on global warming from methane and tropospheric ozone from hydrogen was conducted, revealing GWP100 values of 0–9.8 with a central value of 4.3 with 95% confidence (Derwent (2018))<sup>14</sup>. This means that over a 100-year period, a pulse emission of 1 kg of hydrogen leads to as much global warming as 4.3 kg of CO<sub>2</sub>. A follow-up study with the STOCHEM-CRI model found a GWP100 value of  $5 \pm 1$ <sup>15</sup>. Recent studies have made a step forward in the research of the climate effect of hydrogen emissions by including the combined effects in the troposphere and stratosphere using global 3D models. Using the UKESM1 model with

prescribed hydrogen surface concentrations, a much higher hydrogen GWP100 of  $12 \pm 6$  was estimated<sup>16</sup>. Perturbing hydrogen emissions in a coupled model (GFDL-AM4.1) an indirect radiative forcing of  $0.84 \text{ mWm}^{-2}$  per  $\text{Tg yr}^{-1}$  hydrogen emitted was estimated; mostly due to longer methane lifetime and increased stratospheric water vapor production<sup>17</sup>. This indirect forcing translated into a GWP100 of  $12.8 \pm 5.2$  (90% confidence interval)<sup>13</sup>. A new analysis with the 2D model TROPOS, which reconciled the values of 2D and 3D models found a GWP100 of  $8 \pm 2$  with 95% confidence<sup>18</sup>.

Here, we present new estimates of the GWP100 of hydrogen, using five global atmospheric chemistry models (GFDL, OsloCTM, INCA, WACCM, and UKCA). We calculate GWP100 using a steady-state perturbation approach that takes all effects of atmospheric hydrogen into account in a comprehensive way. The models are forced by present-day (2010) hydrogen and methane surface concentrations. As idealized experiments, we perturb the models with 10% increase in hydrogen and methane surface concentrations, respectively, and combine the results to derive the full chemical response of perturbing hydrogen emissions. This approach allows us to assess separate uncertainties in the terms used to derive the GWP, and thus give us a better estimate of the overall uncertainty. Two models (OsloCTM and GFDL) also contribute simulations driven by hydrogen emissions and deposition fluxes instead of fixed surface concentrations of hydrogen and give similar results, confirming our understanding of chemical feedbacks that occur in emissions-driven simulations.

## Results

**The hydrogen budget.** Figure 1 shows the hydrogen budget as simulated by six models (GFDL, OsloCTM, INCA, UCI, UKCA, and WACCM). The burden of hydrogen is close to 200 Tg (a) and the total lifetime of hydrogen is 2.4 years (1.9–2.7 years model range) (b). The chemical production and loss of hydrogen in the atmosphere are shown in (c). There is a very good agreement between the models on the chemistry of hydrogen, despite the models being quite different. One exception is WACCM, which has lower formaldehyde levels in the troposphere compared to the other models. In our model set-up for prescribed surface concentrations, the amount of hydrogen in the atmosphere (a) is determined by the surface concentrations, the chemical production, and loss, but does not get affected by the soil sink or emissions. The models diagnose their own soil sink (see Methods), and this is used together with atmospheric loss, to calculate the lifetime in the models. The corresponding emissions can be estimated as the total sink and the total production must balance. In d) the soil sink and estimated emissions are shown. The soil sink values have a large range between 44–73  $\text{Tg yr}^{-1}$ , while the estimated emissions range between 29–68  $\text{Tg yr}^{-1}$ . The total lifetime is calculated by the burden divided by the soil sink (as diagnosed in the models) and atmospheric loss, which is equal to the total loss, as it will be in steady state.

**Atmospheric composition changes.** To investigate the impact of hydrogen on the atmospheric composition, we have perturbed the models (relative to 2010 levels) with a 10% increase in hydrogen surface concentrations (PERT\_H2). Because methane is also fixed at the surface we perform an additional experiment, a 10% increase in methane at the surface (PERT\_CH4) to indirectly diagnose the impact of hydrogen via methane changes on the atmospheric composition.

By increasing the hydrogen surface concentration by 10%, the models show consistent changes in atmospheric composition. Figure 2 shows the zonal annual mean changes due to hydrogen in OH, methane, water vapor, and ozone from the surface up to 1 hPa.

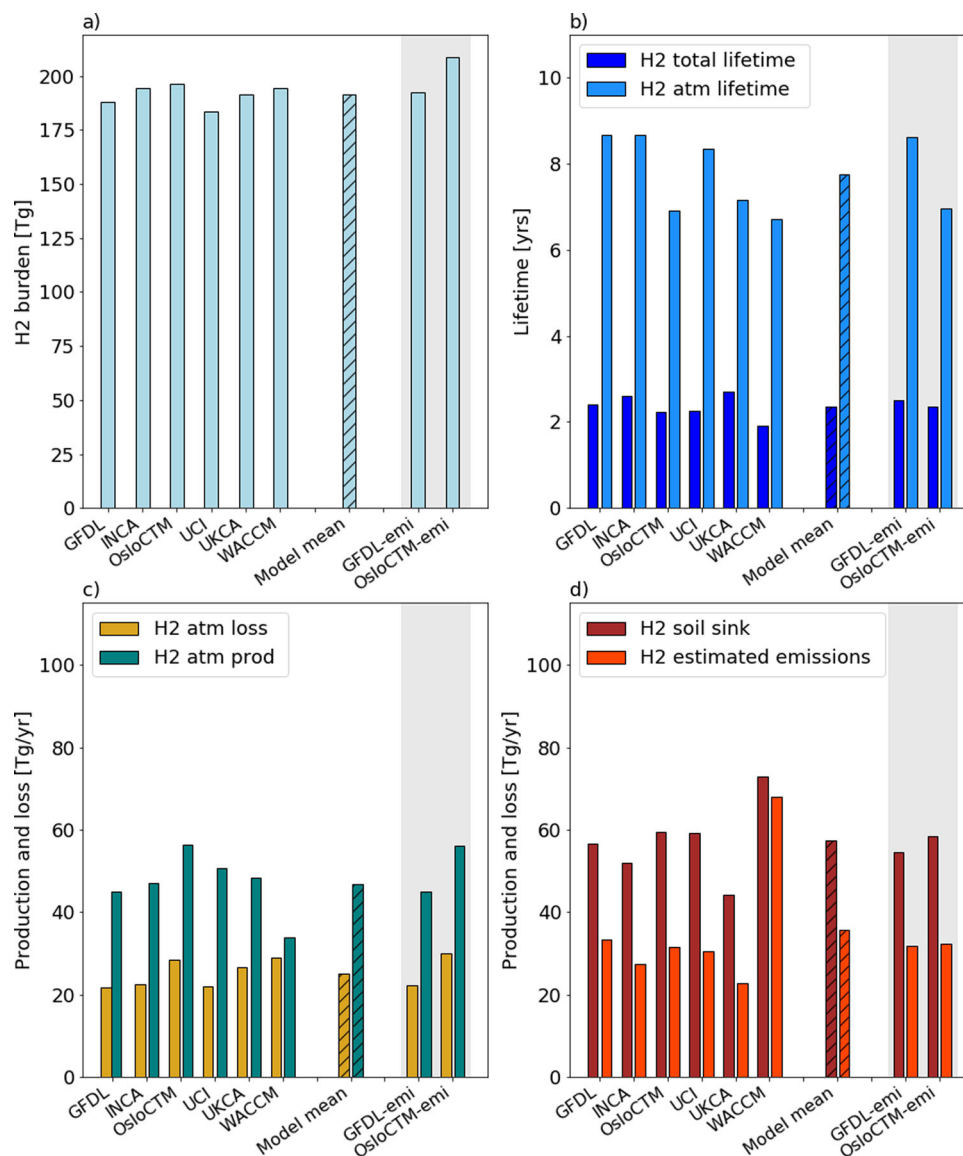


**Fig. 1 The hydrogen budget.** The hydrogen budget terms for all the models; **a** total burden (in Tg), **b** total lifetime and atmospheric lifetime (in years), **c** atmospheric chemical loss and atmospheric chemical production (in  $\text{Tg yr}^{-1}$ ), and **d** soil sink and estimated emissions (soil sink + atm. loss - atm. production) (in  $\text{Tg yr}^{-1}$ ). The model mean is based on the six models with prescribed surface concentrations of hydrogen (left side). The hydrogen budget is also presented in Supplementary Table 1.

Methane-induced changes were included by scaling results from the methane experiment to the expected methane change in the hydrogen experiment (see Supplementary Fig. 2).

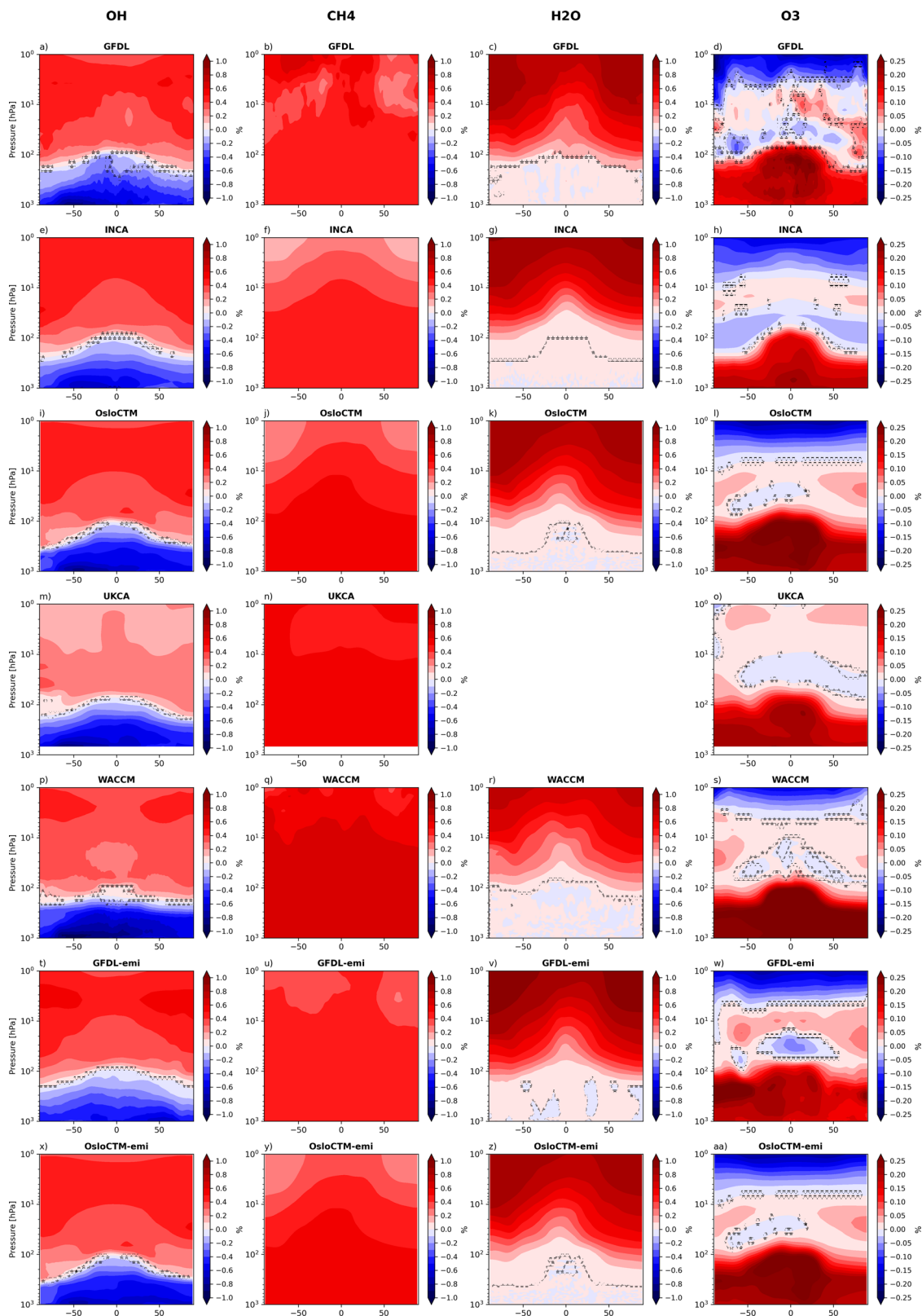
In the troposphere, all models show a decrease in OH resulting in increased levels and longer lifetime of methane. The reduction in OH also causes an increase in  $\text{HO}_2$ , leading to increased production of tropospheric ozone. Previous studies have shown a large spread in effects on ozone layer depletion, ranging from up to 10% in specific areas and under extreme adaption and leakage scenarios<sup>19–21</sup> to minor changes including small increases<sup>22,23</sup>. Here, in the lower stratosphere at levels between 100 and 10 hPa, the models all show only small changes to the ozone layer (Fig. 2).

The oxidation of hydrogen higher up in the dry stratosphere increases water vapor concentrations there due to a much longer lifetime than in the troposphere, causing a cooling effect in the stratosphere and an increased greenhouse effect<sup>24</sup>.

**Radiative forcing.** Figure 3 illustrates and summarizes the radiative forcing effects of increasing hydrogen. Each bar shows global mean

effective radiative forcing (ERF) due to one Tg flux of hydrogen, for each model. Here, the model results are normalized by the change in the hydrogen flux in the perturbed simulations (the emissions needed to sustain the concentration perturbation and hence include chemical feedbacks) and the contribution to ERF via methane changes added (see Method and Supplementary Table 3).

Increased hydrogen in the atmosphere leads to higher methane levels. This gives an ERF from methane (green bars) of  $0.46 \text{ mW m}^{-2}$  ( $0.39\text{--}0.51 \text{ mW m}^{-2}$  model range) per flux hydrogen ( $\text{Tg yr}^{-1}$ ). The methane increase changes both ozone and stratospheric water vapor in addition to the direct changes in ozone and stratospheric water vapor by increased hydrogen. Both these effects are included in Fig. 3. An increase in methane increases its own lifetime<sup>25,26</sup>. The simulated methane feedback factor ranges from 1.36 to 1.55 (Supplementary Table 2) which is a bit high compared to other multi-model studies  $1.34 \pm 0.06$ <sup>26</sup> and  $1.30 \pm 0.07$ <sup>27</sup>. Our estimated hydrogen feedback is slightly negative, and the factor ranges from 0.95 to 1.0 (Table S01). These feedbacks are also included in Fig. 3.



We have calculated the ozone radiative forcing by using a monthly three-dimensional kernel for ozone radiative forcing<sup>28</sup> in the two perturbation experiments relative to the control run. This results in a total ozone ERF of 0.40 (0.28–0.48)  $\text{mW m}^{-2}$  per  $\text{Tg yr}^{-1}$  of hydrogen flux (yellow bars).

In the stratosphere, hydrogen increases water vapor production. We have calculated the radiative forcing for stratospheric

water vapor offline, using separate radiative transfer schemes for longwave and shortwave radiation, including stratospheric temperature adjustments. This results in a stratospheric water vapor ERF of 0.19 (0.08–0.29)  $\text{mW m}^{-2}$  per  $\text{Tg yr}^{-1}$  of hydrogen flux (purple bars).

Sulfate ( $\text{SO}_4$ ) aerosols are formed through gas phase oxidation of  $\text{SO}_2$  by OH, but also through aqueous phase reaction of  $\text{SO}_2$



**Fig. 2 Changes in atmospheric composition.** Relative changes (in %) in zonal mean concentrations of OH (first column), CH<sub>4</sub> (second column), H<sub>2</sub>O (third column), and O<sub>3</sub> (fourth column) due to a 10% increase in hydrogen for all models; GFDL (a–d), INCA (e–h), OsloCTM (i–l), UKCA (m–o), WACCM (p–s), GFDL-emi (t–w), and OsloCTM-emi (x–aa). This is done by comparing PERT\_H2 (Supplementary Fig. 1) plus the contributions from the change in methane caused by hydrogen in PERT\_CH4 (scaled to match the methane change in PERT\_H2), to CTRL (Supplementary Fig. 2). In the GFDL-emi experiment this combination was performed within the experiment directly, which is what is plotted here. The UKCA model used, did not model stratospheric water vapor changes. Black dots mark areas where changes between the control and perturbed run are not significant. Significance is here defined as 95% or more of the points with same latitude and height agree on the sign of the change. Because of different perturbation magnitudes in GFDL-emi, GFDL, and OsloCTM-emi, these models have been scaled by 25, 4, and 1.65, respectively, to match the 10% perturbation in the hydrogen surface concentrations in the other models (see Methods).

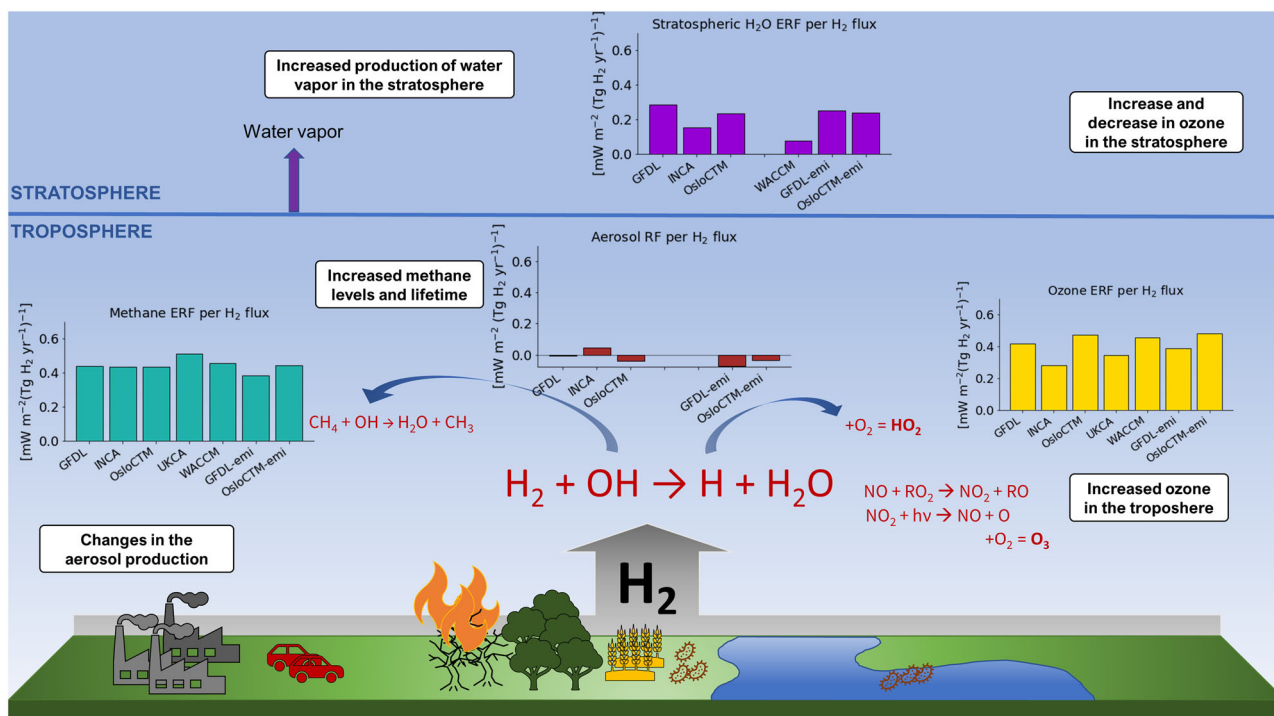


**Fig. 3 Changes in the radiative forcing due to 1 Tg flux of hydrogen.** The main changes in the radiative forcing due to 1 Tg flux of hydrogen; methane (green bars), ozone (yellow), stratospheric water vapor (purple), and aerosols (red). The values are presented in Supplementary Table 3.

with ozone and H<sub>2</sub>O<sub>2</sub> (involving many different chemical species)<sup>29,30</sup>. It is therefore not obvious that a reduced OH level from hydrogen emissions leads to less sulfate aerosols. INCA and OsloCTM have a general reduction in sulfate from hydrogen emission whereas the sign of global sulfate burden varies in the GFDL model. The changes in aerosols give rise to additional radiative forcing via aerosol-radiation-cloud interactions. We have therefore calculated the direct and first indirect radiative forcing of aerosols for the models where this was possible, shown as red bars in Fig. 3. In OsloCTM the global mean burden of sulfate decreases from hydrogen emissions, but aqueous phase reactions lead to more sulfate aerosols at low altitudes leading to a strengthening in the indirect aerosol effect and overall negative forcing. In all model simulations the aerosol forcing is weak (see Fig. 3) and for all experiments, it is weaker in magnitude compared to the change in stratospheric water vapor.

Supplementary Table 3 summarizes the main effects of increasing hydrogen in the atmosphere normalized by 1 Tg flux of hydrogen.

**Global warming potential.** GWP100 for hydrogen is the ratio of the absolute global warming potential (AGWP100) for hydrogen relative to that for CO<sub>2</sub>. AGWP100 is defined as the time-integrated radiative forcing to a 1 kg pulse emission of a gas over 100 years. Since hydrogen perturbs many gases, we have summed

all forcing contributions, assuming that all perturbations from the initial hydrogen pulse have decayed, so the steady-state calculation will match the integrated transient (see Methods). Figure 4 shows the hydrogen GWP100 values for all models, split into the contribution from methane, ozone, and stratospheric water vapor. The model mean hydrogen GWP100 is  $11.6 \pm 2.8$  (one standard deviation). The largest contribution is from changes in methane (44%), followed by ozone (38%) and stratospheric water vapor (18%). The reported GWP100 does not include any aerosol effects which are consistent with IPCC reporting. The number  $11.6 \pm 2.8$  (one standard deviation) is comparable to Warwick et al.<sup>16</sup> ( $12 \pm 6$ ) and Hauglustaine et al.<sup>13</sup> ( $12.8 \pm 5.2$ , 90% confidence interval), but twice as high as previously published numbers<sup>14,15</sup> which did not consider changes in the stratosphere. The GWP100 values for each component are provided in Supplementary Table 6. In this study we report GWP100 as it is the official emission metric for United Nations Framework Convention on Climate Change (UNFCCC). We have also calculated other time horizons; GWP20 ( $37.3 \pm 15.1$ ) and GWP500 ( $3.31 \pm 0.98$ ) (Supplementary Table 8). By reducing short-lived climate forcers (SLFCs), such as hydrogen, there is potential to slow down global warming in the next 20–25 years. GWP20 is relevant for shorter time horizons, but it might overestimate the impact of SLFCs over CO<sub>2</sub>, as GWP is an integrated metric, and not an end-point metric<sup>31,32</sup>. Since the main focus of a hydrogen

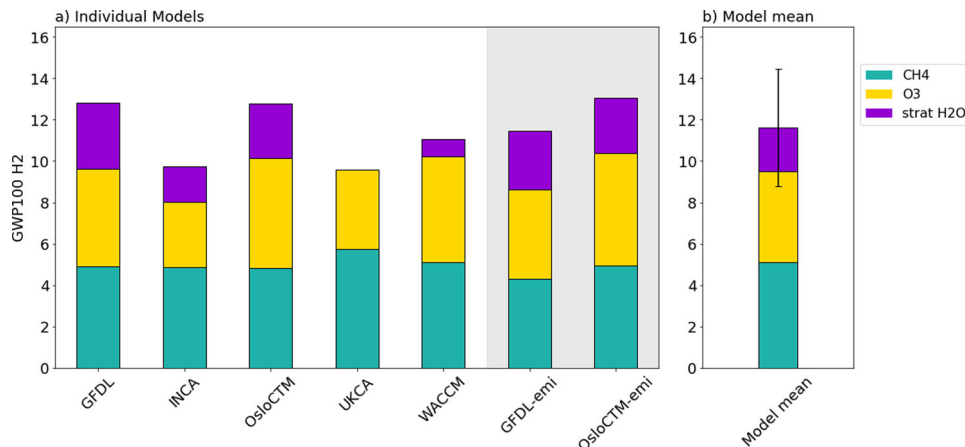


**Fig. 4 The GWP100 of hydrogen.** Hydrogen GWP100 for the individual models (a) and model mean (b), split into contributions from methane (green), ozone (yellow), and stratospheric water vapor (purple). The UKCA model only includes tropospheric changes. The uncertainty range in (b) is calculated using the model mean and spread in underlying values found in literature and the model ensemble spread. Details on the calculation can be found in Methods.

**Table 1 Uncertainties in the GWP100 calculation.**

Component	Percentage uncertainty in the GWP100 best estimate due to:			
	Absolute uncertainty 1σ	Absolute uncertainty 90% confidence	Percent contribution to GWP uncertainty	Source for underlying spread
Total	± 2.8	± 4.7	24	
AGWP <sub>CO<sub>2</sub></sub> ( $\sigma_{AGWP_{CO_2}}$ )	$\frac{W_{yr}}{m^2 \cdot kg}$ ± 1.4 · 10 <sup>-14</sup>	± 2.3 · 10 <sup>-14</sup>	16	48
H <sub>2</sub> burden change ( $\sigma_{\Delta Burden_{H_2}}$ )	$\frac{Tg}{yr}$ ± 0.17	± 0.29	0.9	Model ensemble
H <sub>2</sub> feedback factor ( $\sigma_{ff_{H_2}}$ )	± 6.3 · 10 <sup>-3</sup>	± 1.0 · 10 <sup>-2</sup>	0.6	Model ensemble
Soil sink ( $\sigma_{soil_{sink}}$ )	$\frac{Tg}{yr}$ ± 15	± 25	18	Expert judgment based on literature (ref. 5 and 17)
Atmospheric loss of H <sub>2</sub> ( $\sigma_{atm_{loss}}$ )	$\frac{Tg}{yr}$ ± 3.0	± 5.0	3.7	Model ensemble
Radiative efficiency of CH <sub>4</sub> ( $\sigma_{r_{CH_4}}$ )	$\frac{W}{m^2 \cdot ppb}$ ± 7.7 · 10 <sup>-5</sup>	± 1.3 · 10 <sup>-4</sup>		33
Direct change in CH <sub>4</sub> concentrations ( $\sigma_{\Delta CH_4_{dir}}$ )	$\frac{Tg}{yr}$ ± 1.1	± 1.8	1.2	Model ensemble
CH <sub>4</sub> feedback factor ( $\sigma_{ff_{CH_4}}$ )	± 0.07	± 0.12	0.1	27
Forcing changes in stratospheric H <sub>2</sub> O ( $\sigma_{AGWP-\tau-H_2O}$ )	$\frac{W}{m^2 \cdot kg}$ ± 2.0 · 10 <sup>-2</sup>	± 3.4 · 10 <sup>-2</sup>	0.04	Model ensemble
Forcing changes in stratospheric O <sub>3</sub> ( $\sigma_{AGWP-\tau-O_3}$ )	$\frac{W}{m^2 \cdot kg}$ ± 1.2 · 10 <sup>-2</sup>	± 1.9 · 10 <sup>-2</sup>	0.02	Model ensemble

The percentage uncertainties are calculated using the same method as Table 7SM.8 of ref. 47, meaning that each percentage contribution is root square summed. We present 1σ uncertainties (68% confidence interval) in addition to the 90% confidence interval assuming a symmetric soil sink uncertainty. We also present the full absolute uncertainty and the source we used to estimate the uncertainty. Where the model ensemble is listed, we have used the standard deviation of the variable from our model ensemble, otherwise, the literature source for the uncertainty estimate is listed. Similar tables for GWP20 and GWP500 can be found in Supplementary Tables 9 and 10.

economy is the reduction of CO<sub>2</sub> emissions in order to achieve the Paris Agreement’s long-term climate target, the use of a short time-horizon may appear less relevant for hydrogen compared to other SLCFs.

Our model ensemble allows us to extend the assessment of uncertainties. To estimate the uncertainties in the GWP100 value to 2.8, we have performed a standard error propagation using model ensemble values and published literature values (as detailed in Methods and Table 1). The largest uncertainty in the estimate of GWP100 of hydrogen is the soil uptake, which is also the largest term in the hydrogen budget, accounting for as much as 80% of the loss of hydrogen<sup>4,5</sup>. If all other factors were known with full certainty, it alone would contribute an uncertainty of ±2.1 (assuming a standard deviation on the soil sink of ±15 Tg yr<sup>-1</sup> based on published soil sink values<sup>5,17</sup> and

our model spread). Note, however, that the uncertainty linked to the AGWP of CO<sub>2</sub> is comparable in size—a contribution of ±1.8 to the uncertainty, if it were the sole source of uncertainty. The uncertainty in atmospheric loss of hydrogen due to OH is the third largest term, and accounts for ±0.43 when considered on its own.

Following the same method as for hydrogen, we can calculate GWP100 for methane. Our model ensemble has a methane GWP100 of 26.6 (23–33 model range) (Supplementary Fig. 3), comparable to the IPCC AR6 values GWP100 of 27.0 ± 11 (90% confidence interval)<sup>33</sup>. The model mean methane perturbation lifetime is 10.4 years (Supplementary Table 2) which is lower than the IPCC AR6 assessed value of 11.8 years<sup>33</sup> but within the uncertainty of 1.8 years. A higher perturbation lifetime will enhance the methane GWP value.

## Discussion

The largest uncertainty in the estimate of GWP100 of hydrogen is the soil sink. This removal is modulated by soil temperature, soil moisture, and the activity of hydrogen-oxidizing bacteria<sup>34–36</sup>. Published global soil removal numbers range from 55 to 88 Tg yr<sup>-1</sup><sup>17,37</sup>, and future work should narrow down this large uncertainty. Current global atmospheric models treat this soil removal in a simplified way and need a more sophisticated treatment of soil sink, but it is limited by the resolution. One way to narrow the uncertainty range in the soil sink would be to get a better estimate of the other sources and sinks of hydrogen.

In our model set-up, the models diagnose their own soil sink to be used in estimating the lifetime. A high soil sink will be compensated for by a large estimate of hydrogen emissions, as is apparent in Fig. 1 for WACCM (73 Tg yr<sup>-1</sup>), which is outside the range of bottom-up estimates (53.5–60 Tg yr<sup>-1</sup>) (Table 1 in ref. 17). The resulting estimated emissions in WACCM (68.1 Tg yr<sup>-1</sup>) are far outside the range in Paulot et al.<sup>17</sup> of 32.3 (29.9–37.1) Tg yr<sup>-1</sup> and other published estimates of 28–48 Tg yr<sup>-1</sup> (Table 1 in<sup>17</sup>). On the other hand, UKCA has a relatively low soil sink of 44 Tg yr<sup>-1</sup>, and the resulting estimated emissions are 23 Tg yr<sup>-1</sup>, also outside the range of published values. However, uncertainties in estimates of hydrogen emissions are not assessed and could be larger than the range of published studies. For instance, one study indicates that geological processes may release over 30 Tg yr<sup>-1</sup> of hydrogen<sup>3</sup>. For a mid-value of published emission estimates of 38 Tg yr<sup>-1</sup> and using the model mean atmospheric chemical production and loss in Fig. 1c (in which there is a good model agreement), the mean soil sink would be 59 Tg yr<sup>-1</sup>. This is close to the model mean soil sink (57 Tg yr<sup>-1</sup>). Since the models employ different soil sink schemes, we have also estimated the GWP100 of hydrogen by using this harmonized soil sink value of 59 Tg yr<sup>-1</sup> in all models. This leads to a GWP100 of hydrogen of 11.4 ± 2.8 (Supplementary Tables 7 and 11) close to the model mean of 11.6 ± 2.8 with the models' own soil sinks.

Our results are derived by perturbing the surface concentration of hydrogen. To assess the sensitivity of our results to this setup, we also perform emission perturbations using the GFDL and OsloCTM models. In GFDL-emi, GFDL has been perturbed with 200 Tg yr<sup>-1</sup> anthropogenic hydrogen emissions, fully coupled for 50 years (as described in<sup>17</sup>). We have also run OsloCTM with the same emissions files as used in GFDL (OsloCTM-emi) in the control run, but with a smaller perturbation (14 Tg yr<sup>-1</sup>) in the perturbed run. The emission-driven runs are also a test on the location of the perturbation, as anthropogenic emissions are perturbed with most of the emissions occurring in the NH, compared to the surface hydrogen concentration perturbation, which means that a lower radiative forcing is expected since the lifetime of hydrogen is shorter in the NH. We have tested the GFDL model with various strengths of perturbations, and there is linearity in the perturbations. For both models, atmospheric changes and GWP of hydrogen are very similar between the hydrogen emission-driven and the hydrogen concentration-driven models. Future work should test for emission location dependency, especially NH vs. SH, aviation altitude, and ocean vs. land.

We have calculated GWP100 by assuming that all perturbations from the initial hydrogen pulse have decayed, so the steady-state calculation will match the integrated transient. A major advantage of assembling the GWP from the component terms is that each term represents a fundamental response of atmospheric chemistry to the hydrogen and methane perturbations, and we can compare these across models. Further, from the model range in individual terms we can assess and identify uncertainties in each, allowing us to propagate an uncertainty in GWP that is

more than just the range in model GWPs. A notable disadvantage in calculating successive perturbations in this way is ensuring that the higher-order terms become small, and that we have identified all the major chemical couplings. Thus, it will be important to do atmospheric chemistry-model calculations as full emissions-driven calculations for methane and to ensure that our separation of the problem into two constrained calculations has not missed any important chemical couplings.

We have run the models with present-day background levels of NO<sub>x</sub>, methane, and CO. These levels are likely to change in the future and may also influence the climate impacts of hydrogen, making it stronger or weaker. For instance, Warwick et al.<sup>16</sup> finds that a reduction in CO, NO<sub>x</sub>, and VOC emissions alongside increases in hydrogen leads to smaller increase in methane due to a reduction in OH, but that the total response is complex and strongly scenario dependent. Future work should explore these dependencies further, including changes in co-emitted species and air pollution by switching to a hydrogen economy.

By using an ensemble of models with detailed forcing calculations, taking all effects into account including the stratosphere, we have found that the GWP100 of hydrogen is twice as high as earlier estimates, and comparable to recent estimates<sup>13,16</sup>. Our estimated GWP100 of hydrogen is 39% of that to fossil fuel methane GWP100 in AR6<sup>33</sup>. This emission metric can be used in various mitigation policy decisions, by comparing different GHG reduction measures, or life cycle analysis. The potential benefit of switching to a hydrogen economy will depend on hydrogen leakage rates and potential reductions in CO<sub>2</sub> emissions and co-emitted species. Various assumptions and estimates of hydrogen leakages vary from 1–10% depending on how hydrogen is being produced, transported, and stored<sup>22,38–40</sup>. The little data that exists on hydrogen leakages comes from assessments and simulations rather than direct measures. Hydrogen leakages will lead to global warming, and it will be important to keep these leakages at a minimum to accomplish the benefits of switching to a hydrogen economy. Therefore, it will be important to develop instruments for leakage detection for monitoring, so we can get a better picture of how large these leakages are today.

## Methods

**Model simulations.** For calculations of GWP from steady state and to investigate changes in atmospheric composition due to increased hydrogen, we ran three sets of simulations:

CTRL: A control simulation with present-day atmospheric composition, where hydrogen and methane surface concentrations (mole fraction) are fixed.

PERT\_H2: As CTRL but the surface concentration of hydrogen is increased by +10%.

PERT\_CH4: As CTRL but the surface concentration of methane is increased by +10%.

From the PERT\_H2 simulation, the change in atmospheric composition and radiative forcing directly due to the increase in hydrogen can be calculated. As the methane concentration is fixed at the surface in these simulations, we need the additional methane experiment, PERT\_CH4, to calculate the change in atmospheric composition and radiative forcing due to the change in the methane lifetime in PERT\_H2.

Five models (see model description below and Table 2) have run these simulations with prescribed hydrogen and methane concentrations at the surface. Above this model layer, hydrogen and methane are treated as chemically reactive tracers in the atmosphere. Additional simulations were also performed with two models that were run with hydrogen emissions instead of fixed surface concentration fields. The methane concentrations were fixed at the surface. GFDL-emi was perturbed with an extra 200 Tg yr<sup>-1</sup> anthropogenic hydrogen emissions and ran for 50 years. The methane surface concentration was increased based on the impact of hydrogen onto OH as estimated from a pure hydrogen perturbation run as described in<sup>17</sup>. OsloCTM-emi ran with the same emissions files as used in GFDL-emi, but with a smaller perturbation of 14 Tg yr<sup>-1</sup> (a doubling of the anthropogenic emissions). Note that for OsloCTM-emi, the hydrogen at the surface, and hence also burden, is slightly larger in CTRL compared to the prescribed fields used in the concentration-driven run. The increase in methane

**Table 2 The model set-up.**

Short name	Long name	Resolution	Experiments	Meteorology	Simulation length (average period)
GFDL	GFDL-AM4.1	-100 kms with 49 vertical levels	i) present-day control run with fixed H <sub>2</sub> surface concentrations ii) 25% increase in H <sub>2</sub> surface concentrations iii) same as ii) but with 40% increase iv) 10% increase in CH <sub>4</sub> surface concentrations	Winds nudged to NCEP 6 hr wind speeds	20 years (last 10 years)
GFDL-emi	GFDL-AM4.1	-100 kms with 49 vertical levels	i) present-day control run with H <sub>2</sub> emissions ii) 200 Tg yr <sup>-1</sup> H <sub>2</sub> emissions and surface CH <sub>4</sub> is increased from 1808 ppbv to 2005 ppbv.	Model's own	50 years (30)
INCA	LMDz-INCA-ORCHIDEE	2.5° × 1.25° with 39 vertical levels	i) present-day control run with fixed H <sub>2</sub> surface concentrations ii) 10% increase in H <sub>2</sub> surface concentrations, iii) 10% increase in CH <sub>4</sub> surface concentrations	ECMWF ERA-5	20 years (3)
OsloCTM	OsloCTM3	-2.25 × 2.25° with 60 vertical levels	i) present-day control run with fixed H <sub>2</sub> surface concentrations ii) 10% increase in H <sub>2</sub> surface concentrations iii) 10% increase in CH <sub>4</sub> surface concentrations	ECMWF OpenIFS 3 hr forecast data	20 years (1)
OsloCTM-emi	OsloCTM3	-2.25 × 2.25° with 60 vertical levels	i) present-day control run with H <sub>2</sub> emissions ii) 14 Tg yr <sup>-1</sup> increase in H <sub>2</sub> emissions. (the results from (iii) in OsloCTM is used for the sensitivities due to a methane flux).	ECMWF OpenIFS 3 hr forecast data	25 years (1)
UCI CTM	UC Irvine CTM	-1,1° × 1,1° grid	i) present-day control run with fixed H <sub>2</sub> surface concentrations	ECMWF OpenIFS 3 hr forecast data	7 years (1)
UKCA	UKESM-AMIP, UKCA vn11.1	1.250° × 1.875° with 85 vertical levels	i) present-day control run with fixed H <sub>2</sub> surface concentrations ii) 10% increase in H <sub>2</sub> surface concentrations iii) 10% increase in CH <sub>4</sub> surface concentrations	Model's own	14 years (1)
WACCM	WACCM6	1.875° × 2.5° with 88 vertical levels	i) present-day control run with fixed H <sub>2</sub> surface concentrations ii) 10% increase in H <sub>2</sub> surface concentrations iii) 10% increase in CH <sub>4</sub> surface concentrations	Model's own	18 years (5)

induced effects by hydrogen was estimated using sensitivities from PERT\_CH4 from the concentration-driven OsloCTM runs.

**Model setup.** The CTRL simulation uses present-day hydrogen surface abundances. The hydrogen surface concentration field used by all models is on monthly resolution and on a zonally averaged one-degree resolution. The field was generated using data from <https://www.esrl.noaa.gov/> using data from 67 stations. The open data includes monthly averages between 1989 and 2005. The data availability varies from station to station, so to create the averaged field we used average monthly values for each month for each station. For each month those averages were fed into a LOWESS smoothing function with fractional smoothing of 0.5 to create a smooth zonal field. Zonal surface field of methane is from input4mip<sup>41</sup> for year 2010. Anthropogenic emissions are from the Community Emissions Data System (CEDS) (version 2017-05-18 as used in CMIP6) for year 2010 and biomass burning as in CMIP6<sup>42</sup>. Natural emissions are the models' own choice.

The models have either run with meteorological fields or with nudged meteorology. In GFDL, a higher perturbation is used due to weaker nudging. See Table 2 for details of the individual model set up and model description below.

**Radiative forcing calculations.** Because methane is held fixed in PERT\_H2, the experiment with 10% increase in methane surface concentrations (PERT\_CH4)

allows us to estimate the impact of hydrogen on surface concentrations of methane. From CTRL and PERT\_H2 we directly diagnose the loss of methane through the CH<sub>4</sub> + OH reaction, and the lifetime of methane due to OH, combined with a lifetime of 240 years for loss in the stratosphere (excluding OH loss) and 160 years for soil sink<sup>43</sup>. The total lifetime of methane in CTRL and PERT\_H2 can be calculated. The methane flux (i.e. the emissions needed to sustain the concentrations) is calculated as the burden divided by the total methane lifetime in each simulation. The difference in the methane flux between PERT\_H2 and CTRL is the additional methane flux for a 10% increase in the surface concentration of hydrogen. The difference in the flux between PERT\_CH4 and CTRL is the flux needed to sustain the 10% increase in methane, and this flux includes the feedback factor. Both the methane and hydrogen feedback factor can be calculated as the perturbation lifetime divided by the total lifetime. The increased concentration of methane in PERT\_H2 that would have occurred (at equilibrium) if it had not been held fixed (e.g.<sup>43</sup>), is then calculated by combining the change in surface concentrations of methane per methane flux (ppb (CH<sub>4</sub>) (Tg(CH<sub>4</sub>) yr<sup>-1</sup>)<sup>-1</sup>) in PERT\_CH4 with the calculated methane flux in PERT\_H2. The methane radiative forcing is calculated by the increase in surface concentration converted using a concentration-to-forcing factor of 0.448 mW m<sup>-2</sup> ppb<sup>-1.44</sup> and adjustment term of -14%<sup>33</sup> to calculate Effective Radiative Forcing (ERF). While Supplementary Table 3 summarizes the total changes in atmospheric composition and effective radiative forcing due to hydrogen, Supplementary Table 4 and Supplementary



Table 5 summarize the changes in atmospheric composition and effective radiative forcing due to hydrogen only (PERT\_H2-CTRL), and methane only (PERT\_CH4-CTRL), respectively.

For total ozone, stratospheric water vapor, and aerosols, radiative forcing is calculated offline for the PERT\_H2 and PERT\_CH4 relative to CTRL.

The ozone radiative forcing is calculated from the changes in the monthly mean three-dimensional ozone fields in the perturbations compared to the control simulation multiplied by a monthly three-dimensional kernel for ozone radiative forcing<sup>28</sup>. As in IPCC AR6, we do not add any adjustments and use the radiative forcing values as ERF.

For stratospheric water vapor, the radiative forcing is calculated offline consistently for all models using separate radiative transfer schemes for longwave and shortwave radiation<sup>45</sup>. Stratospheric temperature adjustment is included in the radiative transfer calculations. There are limited studies for adjustment of methane-induced changes in stratospheric water vapor, and the IPCC AR6 presented an adjustment less than 1 with low confidence. We choose to treat the RF values here as ERF.

Direct aerosol effect and indirect aerosol effect is calculated offline<sup>46</sup>. For the indirect aerosol effect only the change in effective radius is simulated. Thus, no rapid adjustment to microphysical properties such as liquid water content or cloud fraction is taken into account. For aerosols we report RF and not ERF.

**Calculation of fluxes and budgets.** For calculations of AGWP we calculated the hydrogen flux needed to sustain the 10% increase in surface concentrations of hydrogen. As for methane, this is calculated as the difference in the flux (lifetime divided by the burden) in PERT\_H2 and CTRL. The models calculate the atmospheric production and loss, but soil sink and emissions are not needed in the simulations, as the hydrogen at the surface is prescribed. The models do diagnose the soil sink (see Model descriptions below), and this loss in addition to the atmospheric loss is used to calculate the lifetime in the models and hence the estimated flux of hydrogen in the simulations.

The radiative forcing in the PERT\_H2 experiment can then be normalized by the hydrogen flux ( $W\ m^{-2}\ (Tg\ yr^{-1})^{-1}$ ). The indirect forcing via methane is added by normalizing the forcing by the methane flux and multiply by the methane flux per hydrogen flux ( $Tg\ CH_4\ (Tg\ H_2)^{-1}$ ) from the PERT\_H2 experiment.

**GWP calculations.**  $GWP_{H_2}$  is the ratio of the absolute global warming potential (AGWP) for hydrogen relative to that for  $CO_2$ . AGWP is defined as the time-integrated radiative forcing of a 1 kg pulse emission of that gas over a given time horizon. For use in the United Nations Framework Convention on Climate Change (UNFCCC) the GWP is integrated over time horizons of 20 (GWP20), 100 (GWP100), and 500 (GWP500) years. In this study, we focus on GWP100 (values of GWP20 and GWP500 are found in Supplementary).

The GWP100 of hydrogen (following 8.SM.6 from IPCC AR5 [Myhre et al. 2013])<sup>47</sup> is defined as:

$$GWP_{H_2}(100) = \frac{AGWP_{H_2}(100)}{AGWP_{CO_2}(100)} = \frac{\int_0^{100} RF_{H_2}(t) dt}{\int_0^{100} RF_{CO_2}(t) dt} \quad (2)$$

As in AR6, we use the effective radiative forcing (ERF) instead of RF. The AGWP100 of  $CO_2$  is  $0.0895\ 10^{-12}\ W\ m^{-2}\ kg^{-1}\ yr$  from IPCC AR6 Table 7.SM.6<sup>48</sup>. The ERF of hydrogen is the sum of the effective radiative forcing contributions by methane, ozone, and stratospheric water vapor.

We rewrite the AGWP from equation (2) to account for results for a run with a pulse emission of mass  $m_i^{em}$  given in units of  $kg\ yr^{-1}$ .

$$AGWP_i(H) = \frac{1}{m_i^{em}} \int_0^H ERF_i(t) dt \quad (3)$$

Hydrogen does not have a direct radiative forcing, but it has various indirect forcing effects (i.e., methane, ozone, and stratospheric water vapor). These forcing terms (i) are summed:<sup>49</sup>

$$AGWP_i(H) = \frac{1}{m_i^{em}} \sum_{FC} \int_0^H ERF_{FC}(t) dt \quad (4)$$

Where  $ERF_{FC}(t)$  is the effective radiative forcing for compound FC caused by the pulse of species  $i$  in the model.

Following the transient decay of emissions in a CTM can be difficult as one must keep accurate track of the rise and fall of the chemical species perturbed by hydrogen. The methane chemical mode has a lifetime of 7–14 years, which means integration needs to be performed over 60 years to accurately account for its rise and decay.

The integral over these transients in all species has been demonstrated to be equal to the steady-state pattern of perturbations from constant emissions scaled by the lifetime of the emitted species<sup>50,51</sup>. This is because when a constant emission perturbation has reached steady state, it contains perturbations from pulses of all ages at one time. The pulse integration result is equal to a simple comparison between forcing changes per burden change in steady state runs with control and

constant emission changes scaled with the emitted species lifetime.

$$AGWP_i(H) = \frac{\tau_{H_2}}{\Delta Burden_{H_2}} \sum_{FC} (ERF_{FC}^{ss-Perturbed} - ERF_{FC}^{ss-Control}) \quad (5)$$

Where  $\Delta Burden_{H_2}$  is the burden change between a perturbed and a control run that have both reached steady state, and  $\tau_{H_2}$  is the lifetime in the control run multiplied by a feedback factor to account for the shift in hydrogen lifetime induced by hydrogen changes.

In practice, we use a slightly different, but equivalent expression for the AGWP to calculate it from the experiments. Including the hydrogen feedback factor in the lifetime, means that the AGWP is equal to the steady-state radiative forcing ( $W\ m^{-2}$ ) divided by flux changes ( $Tg\ H_2\ yr^{-1}$ ) needed to sustain the perturbation.

$$AGWP_i(H) = \frac{1}{\Phi_i^{ss-Perturbed} - \Phi_i^{ss-Control}} \sum_{FC} (ERF_{FC}^{ss-Perturbed} - ERF_{FC}^{ss-Control}) \quad (6)$$

Where  $\Phi_i^{ss-Perturbed}$  and  $\Phi_i^{ss-Control}$  are the steady state fluxes of hydrogen in the PERT\_H2 and CTRL runs. In our setup, changes due to methane changes are diagnosed in a separate experiment, which leads to a scaling for methane changes. These correspond to radiative forcing changes between the PERT\_H2 and CTRL and scaled PERT\_CH4 and CTRL experiments respectively.

For uncertainty calculation, we expand the equation in more detail and rewrite the flux changes as burden changes divided by hydrogen lifetime:

$$AGWP_{H_2} = \frac{\tau_{H_2}}{\Delta Burden_{H_2}} \cdot \left[ r_{CH_4} \cdot ff_{CH_4} \cdot \Delta C_{CH_4} + \Delta ERF_{O_3} + \Delta ERF_{H_2O} \right] \quad (7)$$

$\Delta$  denotes changes between the control and perturbed experiments where changes in between PERT\_CH4 and CTRL have been scaled to match the expected changes in methane between PERT\_H2 and CTRL, if the methane had not been fixed at the surface.  $r_{CH_4}$  is the radiative efficiency of methane including rapid adjustments,  $ff_{CH_4}$  is the methane feedback factor, and  $C_{CH_4}$  is the scaled concentration change of methane.

As mentioned above, the longest-lived, climate-relevant perturbations induced by molecular hydrogen emissions, will be those tied to the methane perturbation with an e-fold time of about 12 yr. Thus, for AGWP100, we can assume that all perturbations from the initial hydrogen pulse will have decayed, and the steady-state calculation will match the integrated transient. For AGWP20, however, perturbations tied to methane will still exist after 20 years, and the steady-state approximation is corrected using the time scale of the methane perturbation (see Supplementary Table 8).

**Uncertainty calculations.** To estimate uncertainties in the GWP value, we use equation (7) and perform a standard error propagation. We are specifically interested in errors that are due to uncertainties in the soil sink and atmospheric loss, hence we take advantage of the fact that lifetime is burden divided by loss to rewrite:

$$AGWP_{H_2} = \frac{Burden_{H_2}}{\Delta Burden_{H_2}} \cdot \frac{ff_{H_2}}{Loss_{H_2,soil,sink} + Loss_{H_2,dry,dep}} \cdot \left[ r_{CH_4} \cdot ff_{CH_4} \cdot \Delta C_{CH_4} + \Delta ERF_{O_3} + \Delta ERF_{H_2O} \right] \quad (8)$$

Where we have rewritten the lifetime as the hydrogen burden divided by the loss. Since the lifetime used is the perturbation lifetime, we also need to include the hydrogen feedback factor to keep the equivalence. The first fraction in the expression,  $\frac{Burden_{H_2}}{\Delta Burden_{H_2}}$ , is now the inverse of the relative burden change. We propagate the error terms in the following way:

$$\sigma_{GWP}^2 = GWP^2 \cdot \left[ \left( \frac{\sigma_{AGWP_{CO_2}}}{AGWP_{CO_2}} \right)^2 + \left( \frac{\sigma_{\Delta Burden_{H_2}}}{\Delta Burden_{H_2}} \right)^2 + \left( \frac{\sigma_{ff_{H_2}}}{ff_{H_2}} \right)^2 \cdot \left( \frac{1}{Loss_{H_2}} \right)^2 \cdot \left( \sigma_{soil,sink}^2 + \sigma_{atm,loss}^2 \right) + \left( \frac{1}{\sum_{FC} \Delta RF_{FC}} \right)^2 \cdot \left\{ \left( r_{CH_4} \cdot ff_{CH_4} \cdot \Delta C_{CH_4} \right)^2 \cdot \left[ \left( \frac{\sigma_{r_{CH_4}}}{r_{CH_4}} \right)^2 + \left( \frac{\sigma_{\Delta C_{CH_4}}}{\Delta C_{CH_4}} \right)^2 + \left( \frac{\sigma_{ff_{CH_4}}}{ff_{CH_4}} \right)^2 \right] \right\} + \sigma_{AGWP_{O_3}}^2 + \sigma_{AGWP_{H_2O}}^2 \right] \quad (9)$$

where we have expanded the forcing of methane to include uncertainties in the radiative efficiency  $r_{CH_4}$  and feedback factor  $ff_{CH_4}$ .

We find a total uncertainty of 2.8.

For the terms that do not measure expanded uncertainty, we use the model mean value. For each of the sigma-terms, we use either the standard deviation of the model spread for the model ensemble, or values from literature. Details on the relative contribution to the total uncertainty for each term, and the source for the spread can be found in Table 1 below. For the soil sink specifically, we report a symmetric uncertainty range of  $\pm 15\ Tg\ yr^{-1}$  around our model mean of  $59\ Tg\ yr^{-1}$ . This does not completely cover the interval stated in Ehrlert and Rohrer<sup>5</sup>. If we assume that the interval in Ehrlert and Rohrer<sup>5</sup> of  $60\ \pm_{-30}^{+30}\ Tg\ yr^{-1}$  is a 90% confidence interval (this is not explicitly stated in the paper), the range is well covered by our range, except the highest soil sink values stemming from top-down estimates<sup>5,6,37</sup>. These high soil sink values cannot be covered by our model ensemble without assuming some unknown source, since their chemical production is far higher than we are able to produce. We feel therefore that reporting mainly 1 sigma confidence intervals, is most appropriate, and that some

additional uncertainty towards lower GWP values is likely when reporting larger uncertainty intervals unless the soil sink can be better constrained.

**Model description.** Table 2 gives an overview of the models and how they are set up, and below is a detailed description of the individual models.

**OsloCTM3.** OsloCTM3<sup>52</sup> covers the troposphere and the stratosphere, with comprehensive chemistry in both regions. The model is driven by 3-hourly meteorological forecast data by the Open Integrated Forecast System (OpenIFS, cycle 38 revision 1) at the European Centre for Medium-Range Weather Forecasts (ECMWF) and the horizontal resolution is  $\sim 2.25 \times 2.25^\circ$  with 60 vertical layers ranging from the surface and up to 0.1 hPa. The model includes 174 components (chemical gases and aerosols) and a complex set of photolytic, bi-molecular, tri-molecular, and heterogeneous reactions. The model has aerosol modules for sulfate, nitrate, black carbon, primary organic carbon, secondary organic aerosols, mineral dust, and sea salt (Lund et al. 2018)<sup>53</sup>. Based on estimates of natural and anthropogenic emissions, dry-deposition velocities, wet-deposition for water-soluble species, and solved chemical reactions, changes in the atmospheric composition of the components are calculated. For hydrogen the dry deposition or soil sink scheme used are Sanderson et al.<sup>54</sup> that takes into account soil moisture effect on dry-deposition velocities for different vegetation types, no uptake when snow covers the ground and a reduced rate for cold surfaces according to Price et al.<sup>55</sup>. The dry-deposition values are scaled in the concentration-driven run so that the estimated total emission is  $\sim 32 \text{ Tg yr}^{-1}$  similar to what was used in Paulot et al.<sup>17</sup>. The same deposition scheme and values were used in the emission-driven runs.

**WACCM6.** WACCM6<sup>56</sup> is the whole atmosphere version of the Community Atmosphere Model version 6 (CAM6) run with 88 vertical levels and  $1.875^\circ \times 2.5^\circ$  horizontal resolution. It fully represents the meridional overturning circulation of the stratosphere, as well as full tropospheric and stratospheric chemistry, with interactive oxidants and ozone. The deposition velocity is computed within the land model (each land type separately).

**UCI CTM.** UCI CTM<sup>57</sup> is a flexible global chemistry-transport model that is closely related to the OsloCTM. Presently, it uses ECMWF Integrated Forecast System meteorology in the native T159L60N80 grid ( $\sim 1.1^\circ$ ). The tropospheric chemistry is moderate, with about 30 species, and the stratospheric chemistry uses a 5-species ( $\text{O}_3$ ,  $\text{NO}_y$ ,  $\text{N}_2\text{O}$ ,  $\text{CH}_4$ ,  $\text{H}_2\text{O}$ ) linearized chemistry. The control run is simulated with fixed hemispheric hydrogen concentrations of 500 and 550 ppb in the Northern and Southern hemispheres. Hydrogen is deposited through dry-deposition only over land using a fixed deposition velocity.

**UKCA.** UKCA<sup>58</sup> is a global chemistry-climate model which is the atmospheric component of the Met Office Unified Model. The atmosphere-only version 11.1 of the model was used with 85 vertical levels and  $1.250^\circ \times 1.875^\circ$  horizontal resolution using the UKCA-StratTrop chemistry configuration. The configuration was run with the Chemistry AeroClim option which is a full chemistry version of the model run with aerosol climatologies. The water vapor in the model was held fixed with respect to the chemistry such that any change in the water vapor mass mixing ratio due to chemistry was not applied to the tracer. This version was modified to run with the chemical tracers in UKCA uncoupled from the radiation such that the radiation was calculated from fixed 2010 trace gas mass mixing ratios and not informed by the chemistry. This full uncoupling of the chemistry and radiation means the driving meteorology in all simulations is identical, so that differences between simulations are purely due to the applied changes in hydrogen or methane. As the water vapor was fixed, the change in water vapor due to changes in hydrogen and methane was not calculated in these experiments.

The hydrogen deposition in UKCA is based on the scheme developed by Sanderson, 2003. Deposition velocity is linear with soil moisture in all regions except C4 surface types where the deposition has a quadratic-log dependence with soil moisture and shrub surface types where deposition velocity does not depend on soil moisture.

**LMDz-INCA-ORCHIDEE.** The LMDZ-INCA global chemistry-aerosol-climate model couples online the LMDZ (Laboratoire de Météorologie Dynamique, version 6) General Circulation Model<sup>59</sup> and the INCA (INteraction with Chemistry and Aerosols, version 5) model<sup>60,61</sup>. The interaction between the atmosphere and the land surface is ensured through the coupling of LMDZ with the ORCHIDEE (ORganizing Carbon and Hydrology In Dynamic Ecosystems, version 1.9) dynamical vegetation model<sup>62</sup>. In the present configuration, we use the Standard Physics parameterization of the GCM<sup>63</sup>. The model includes 39 hybrid vertical levels extending up to 70 km. The horizontal resolution is  $1.25^\circ$  in latitude and  $2.5^\circ$  in longitude. The GCM winds are nudged towards ECMWF ERA-5 meteorology for the period 2000–2020 by applying at each time step a correction term to the GCM u and v wind components with a relaxation time of 2.5 h<sup>60,64</sup>. INCA includes a state-of-the-art  $\text{CH}_4$ - $\text{NO}_x$ - $\text{CO}$ - $\text{NMHC}$ - $\text{O}_3$  tropospheric photochemistry<sup>60,65</sup>. Chemical species and reactions specific to the middle atmosphere are also included with chemical species belonging to the chlorine and bromine chemistry<sup>66</sup>. For aerosols, the INCA model simulates the distribution of aerosols with anthropogenic

sources such as sulfates, nitrates, black carbon (BC), organic carbon (OC), as well as natural aerosols such as sea salt and dust. The heterogeneous reactions on both natural and anthropogenic tropospheric aerosols are included in the model<sup>60,61,67</sup>. Ammonia and nitrates aerosols are considered as described by Hauglustaine et al.<sup>61</sup>. Based on Hauglustaine and Ehhalt<sup>68</sup>, the Net Primary Productivity (NPP) is used to constrain the seasonal and geographical distribution of  $\text{H}_2$  dry-deposition velocity in LMDz-INCA. The NPP is provided to INCA as monthly mean data prepared with the ORCHIDEE land surface model.

**GFDL-AM4.1.** GFDL-AM4.1 is the atmospheric component of the Earth-System Model 4.1<sup>69,70</sup> with a horizontal resolution of  $\sim 100 \text{ km}$  with 49 vertical levels. The model is run with two different configurations. In GFDL-emi the model is run with repeating hydrogen emissions over 50 years using 2010 conditions as described in Paulot et al.<sup>17</sup>. In the perturbation experiment the hydrogen anthropogenic emissions are increased by  $200 \text{ Tg yr}^{-1}$  and surface methane concentrations are increased from 1808 ppbv to 2005 ppbv. In GFDL, the model is run with prescribed hydrogen and methane as the other models, with horizontal winds nudged to 6h-wind speeds from NCEP. A greater perturbation is used (+40%) to reduce noise in the stratosphere, where nudging is weak.

## Data availability

Data from the modeling runs described in this paper are available in form of netcdf files with <https://doi.org/10.11582/2023.00024> in the NIRD research data archive: <https://archive.sigma2.no/pages/public/datasetDetail.jsf?id=10.11582/2023.00024>.

## Code availability

Custom code for this paper is available in the form of jupyter notebooks as version v0.1.0 of this code [https://github.com/ciceroOslo/Hydrogen\\_GWP](https://github.com/ciceroOslo/Hydrogen_GWP) on github, released under the Apache-2.0 license.

Received: 17 February 2023; Accepted: 19 May 2023;  
Published online: 07 June 2023

## References

- Novelli, P. C. Atmospheric hydrogen mixing ratios from the NOAA GMD carbn cycle cooperative global air sampling network. 1988–2005 (NOAA/ESRL) (2006).
- Patterson, J. D. et al. Atmospheric history of  $\text{H}_2$  over the past century reconstructed from South pole firn air. *Geophys. Res. Lett.* **47**, e2020GL087787 (2020).
- Zgonnik, V. The occurrence and geoscience of natural hydrogen: a comprehensive review. *Earth-Sci. Rev.* **203**, <https://doi.org/10.1016/j.earscirev.2020.103140> (2020).
- Novelli, P. C. et al. Molecular hydrogen in the troposphere: global distribution and budget. *J. Geophys. Res.* **104**, 30427–30444 (1999).
- Ehhalt, D. H. & Rohrer, F. The tropospheric cycle of  $\text{H}_2$ : a critical review. *Tellus B: Chem. Phys. Meteorol.* **61**, 500–535 (2009).
- Rhee, T. S., Brenninkmeijer, C. A. M. & Röckmann, T. The overwhelming role of soils in the global atmospheric hydrogen cycle. *Atmos. Chem. Phys.* **6**, 1611–1625 (2006).
- Prather, M. J. Time scales in atmospheric chemistry: theory, GWPs for  $\text{CH}_4$  and  $\text{CO}$ , and runaway growth. *Geophys. Res. Lett.* **23**, 2597–2600 (1996).
- Levy, H. Normal atmosphere: large radical and formaldehyde concentrations predicted. *Science* **173**, 141–143 (1971).
- Isaksen, I. S. A. & Dalsøren, S. B. Getting a better estimate of an atmospheric radical. *Science* **331**, 38–39 (2011).
- Prather, M. J. Lifetimes and eigenstates in atmospheric chemistry. *Geophys. Res. Lett.* **21**, 801–804 (1994).
- Sherwood, S. C., Dixit, V., and Salomez, C. The global warming potential of near-surface emitted water vapour. *Environ. Res. Lett.* **13**, 104006 (2018).
- O'Connor, F. M. et al. Apportionment of the pre-industrial to present-day climate forcing by methane using UKESM1: the role of the cloud radiative effect. *J. Adv. Model. Earth Syst.* **14**, e2022MS002991 (2022).
- Hauglustaine, D. et al. Climate benefit of a future hydrogen economy. *Commun. Earth Environ.* **3**, 295 (2022).
- Derwent, R. G. et al. Uncertainties in models of tropospheric ozone based on Monte Carlo analysis: tropospheric ozone burdens, atmospheric lifetimes and surface distributions. *Atm. Env.* **180**, 93–102 (2018).
- Derwent, R. G. et al. Global modelling studies of hydrogen and its isotopomers using STOCHEM-CRI: likely radiative forcing consequences of a future hydrogen economy. *Int. J. Hydrog. Energy* **45**, 9211–9221 (2020).

16. Warwick, N. J. et al. Atmospheric composition and climate impacts of a future hydrogen economy. *Atmos. Chem. Phys. Discuss.* <https://doi.org/10.5194/acp-2023-29> (2023).
17. Paulot, F. et al. Global modeling of hydrogen using GFDL-AM4.1: sensitivity of soil removal and radiative forcing. *Int. J. Hydrog. Energy* **46**, 13446–13460 (2021).
18. Derwent, R. G. Global warming potential (GWP) for hydrogen: sensitivities, uncertainties and meta-analysis. *Int. J. Hydrog. Energy* <https://doi.org/10.1016/j.ijhydene.2022.11.219> (2022).
19. Tromp, T. K. et al. Potential environmental impact of a hydrogen economy on the stratosphere. *Science* **300**, 1740–1742 (2003).
20. Feck, T., Grooß, J.-U., and Riese, M. Sensitivity of Arctic ozone loss to stratospheric H<sub>2</sub>O. *Geophys. Res. Lett.* **35**, <https://doi.org/10.1029/2007GL031334> (2008).
21. Vogel, B., Feck, T., Grooß, J.-U. & Riese, M. Impact of a possible future global hydrogen economy on Arctic stratospheric ozone loss. *Energy Environ. Sci.* **5**, 6445–6452 (2012).
22. van Ruijven, B. et al. Emission scenarios for a global hydrogen economy and the consequences for global air pollution. *Glob. Environ. Change* **21**, 983–994 (2011).
23. Wang, D. et al. Impact of a future H<sub>2</sub>-based road transportation sector on the composition and chemistry of the atmosphere – part 2: Stratospheric ozone. *Atmos. Chem. Phys.* **13**, 6139–6150 (2013).
24. Forster, P. M. de F., and Shine, K. P. Assessing the climate impact of trends in stratospheric water vapor. *Geophys. Res. Lett.* **29**, <https://doi.org/10.1029/2001GL013909> (2002).
25. Prather, M. et al. Atmospheric Chemistry and Greenhouse Gases. Climate Change 2001: The Scientific Basis. 239–287 (2001).
26. Holmes, C. D. et al. Future methane, hydroxyl, and their uncertainties: key climate and emission parameters for future predictions. *Atmos. Chem. Phys.* **13**, 285–302 (2013).
27. Thornhill, G. D. et al. Effective radiative forcing from emissions of reactive gases and aerosols – a multi-model comparison. *Atmos. Chem. Phys.* **21**, 853–874 (2021).
28. Skeie, R. B. et al. Historical total ozone radiative forcing derived from CMIP6 simulations. *Npj Clim. Atmos. Sci.* **3**, <https://doi.org/10.1038/s41612-020-00131-0> (2020).
29. Berglen, T. F. et al. A global model of the coupled sulfur/oxidant chemistry in the troposphere: the sulfur cycle. *J. Geophys. Res. Atmos.* **109**, <https://doi.org/10.1029/2003JD003948> (2004).
30. Pattanyus, A. K., Businger, S. & Howell, S. G. Review of sulfur dioxide to sulfate aerosol chemistry at Kilauea Volcano, Hawai'i. *Atmos. Environ.* **185**, 262–271 (2018).
31. Boucher, O. & Reddy, M. S. Climate trade-off between black carbon and carbon dioxide emissions. *Energy Policy* **36**, 193–200 (2008).
32. Shine, K. P. et al. Alternatives to the global warming potential for comparing climate impacts of emissions of greenhouse gases. *Clim. Change* **68**, 281–302 (2005).
33. Forster, et al. The Earth's Energy Budget, Climate Feedbacks, and Climate Sensitivity. In Climate Change 2021: The Physical Science Basis. Contribution of Working Group I to the Sixth Assessment Report of the Intergovernmental Panel on Climate Change [Masson-Delmotte, V., P. Zhai, A. Pirani, S. L. Connors, C. Péan, S. Berger, N. Caud, Y. Chen, L. Goldfarb, M. I. Gomis, M. Huang, K. Leitzell, E. Lonnoy, J. B. R. Matthews, T. K. Maycock, T. Waterfield, O. Yelekçi, R. Yu, and B. Zhou (eds.)]. Cambridge University Press, 923 Cambridge, United Kingdom and New York, NY, USA, 923–1054 (2021).
34. Conrad, R. & Seiler, W. Influence of temperature, moisture, and organic carbon on the flux of H<sub>2</sub> and CO between soil and atmosphere: Field studies in subtropical regions. *J. Geophys. Res. Atmos.* **90**, 5699–5709 (1985).
35. Constant, P., Poissant, L. & Villemur, R. Tropospheric H<sub>2</sub> budget and the response of its soil uptake under the changing environment. *Sci Total Environ.* **407**, 1809–1823 (2009).
36. Ehhalt, D. H. and Rohrer, F. Deposition velocity of H<sub>2</sub>: a new algorithm for its dependence on soil moisture and temperature. *Tellus B: Chem. Phys. Meteorol.* **65**, <https://doi.org/10.3402/tellusb.v65i0.19904> (2013).
37. Xiao X., et al. Optimal estimation of the soil uptake rate of molecular hydrogen from the advanced global atmospheric gases experiment and other measurements. *J. Geophys. Res.*, **112**, <https://doi.org/10.1029/2006jd007241> (2007).
38. Derwent, R. et al. Global environmental impacts of the hydrogen economy. *Int. J. Nuclear Hydrog. Product. Appl.* **1**, 57–67 (2006).
39. Frazer-Nash Consultancy. Fugitive Hydrogen emissions in a future hydrogen economy. (2022).
40. Schultz, M. G. et al. Air pollution and climate-forcing impacts of a global hydrogen economy. *Science* **302**, 624–627 (2003).
41. Meinshausen, M. et al. Historical greenhouse gas concentrations for climate modelling (CMIP6). *Geosci. Model Dev.* **10**, 2057–2116 (2017).
42. van Marle, M. J. E. et al. Historic global biomass burning emissions for CMIP6 (BB4CMIP) based on merging satellite observations with proxies and fire models (1750–2015). *Geosci. Model Dev.* **10**, 3329–3357 (2017).
43. Stevenson, D. S. et al. Tropospheric ozone changes, radiative forcing and attribution to emissions in the Atmospheric Chemistry and Climate Model Intercomparison Project (ACCMIP). *Atmos. Chem. Phys.* **13**, 3063–3085 (2013).
44. Etmann, M. et al. Radiative forcing of carbon dioxide, methane, and nitrous oxide: a significant revision of the methane radiative forcing. *Geophys. Res. Lett.* **43**, <https://doi.org/10.1002/2016gl071930> (2016).
45. Myhre, G. et al. Radiative forcing due to stratospheric water vapour from CH<sub>4</sub> oxidation. *Geophys. Res. Lett.* **34**, <https://doi.org/10.1029/2006GL027472> (2007).
46. Myhre, G. et al. Multi-model simulations of aerosol and ozone radiative forcing due to anthropogenic emission changes during the period 1990–2015. *Atmos. Chem. Phys.* **17**, 2709–2720 (2017).
47. Myhre, G. et al. Anthropogenic and Natural Radiative Forcing. In: Climate Change 2013: The Physical Science Basis. Contribution of Working Group I to the Fifth Assessment Report of the Intergovernmental Panel on Climate Change. 659–740 (2013).
48. Smith, C. et al. The Earth's Energy Budget, Climate Feedbacks, and Climate Sensitivity. Supplementary Material. In: Climate Change 2021: The Physical Science Basis. Contribution of Working Group I to the Sixth Assessment Report of the Intergovernmental Panel on Climate Change [Masson-Delmotte, V., P. Zhai, A. Pirani, S. L. Connors, C. Péan, S. Berger, N. Caud, Y. Chen, L. Goldfarb, M. I. Gomis, M. Huang, K. Leitzell, E. Lonnoy, J. B. R. Matthews, T. K. Maycock, T. Waterfield, O. Yelekçi, R. Yu, and B. Zhou (eds.)] (Cambridge University Press, 2021).
49. Aamaas, B., Peters, G. P. & Fuglestvedt, J. S. Simple emission metrics for climate impacts. *Earth Syst. Dyn.* **4**, 145–170 (2013).
50. Prather, M. J. Lifetimes of atmospheric species: Integrating environmental impacts. *Geophys. Res. Lett.* **29**, <https://doi.org/10.1029/2002GL016299> (2002).
51. Prather, M. J. Lifetimes and time scales in atmospheric chemistry. *Philos. Trans. Royal Soc. A* **365**, 1705–1726 (2007).
52. Søvdø, O. A. et al. The chemical transport model Oslo CTM3. *Geosci. Model Dev.* **5**, 1441–1469 (2012).
53. Lund, M. T. et al. Concentrations and radiative forcing of anthropogenic aerosols from 1750 to 2014 simulated with the Oslo CTM3 and CEDS emission inventory. *Geosci. Model Dev.* **11**, 4909–4931 (2018).
54. Sanderson, M. G. et al. Simulation of global hydrogen levels using a lagrangian three-dimensional model. *J. Atmos. Chem.* **46**, 15–28 (2003).
55. Price, H. et al. Global budget of molecular hydrogen and its deuterium content: constraints from ground station, cruise, and aircraft observations. *J. Geophys. Res.* **112**, <https://doi.org/10.1029/2006JD008152> (2007).
56. Gettelman, A. et al. The whole atmosphere community climate model version 6 (WACCM6). *J. Geophys. Res.* **124**, 12380–12403 (2019).
57. Prather, M. J. et al. Global atmospheric chemistry—which air matters. *Atmos. Chem. Phys.* **17**, 9081–9102 (2017).
58. Archibald, A. T. et al. Description and evaluation of the UKCA stratosphere–troposphere chemistry scheme (StratTrop v1.0) implemented in UKESM1. *Geosci. Model Dev.* **13**, 1223–1266 (2020).
59. Hourdin, F. et al. LMDZ6A: the atmospheric component of the IPSL climate model with improved and better tuned physics. *J. Adv. Model. Earth Syst.* **12**, <https://doi.org/10.1029/2019MS001892> (2020).
60. Hauglustaine, D. A. et al. Interactive chemistry in the Laboratoire de Météorologie Dynamique general circulation model: Description and background tropospheric chemistry evaluation. *J. Geophys. Res.* **109**, <https://doi.org/10.1029/2003JD003957> (2004).
61. Hauglustaine, D. A., Balkanski, Y. & Schulz, M. A global model simulation of present and future nitrate aerosols and their direct radiative forcing of climate. *Atmos. Chem. Phys.* **14**, 11031–11063 (2014).
62. Krinner, G. et al. A dynamic global vegetation model for studies of the coupled atmosphere–biosphere system. *Glob. Biogeochem. Cycles* **19**, <https://doi.org/10.1029/2003GB002199> (2005).
63. Boucher, O. et al. Presentation and evaluation of the IPSL-CM6A-LR climate model. *J. Adv. Model. Earth Syst.*, **12**, e2019MS002010 (2020).
64. Hourdin, F. & Issartel, J. P. Sub-surface nuclear tests monitoring through the CTBT Xenon network. *Geophys. Res. Lett.* **27**, 2245–2248 (2000).
65. Folberth, G. A. et al. Interactive chemistry in the Laboratoire de Météorologie Dynamique general circulation model: model description and impact analysis of biogenic hydrocarbons on tropospheric chemistry. *Atmos. Chem. Phys.* **6**, 2273–2319 (2006).
66. Terrenoire, E. et al. Impact of present and future aircraft NO<sub>x</sub> and aerosol emissions on atmospheric composition and associated direct radiative forcing of climate. *Atmos. Chem. Phys.* **22**, 11987–12023 (2022).
67. Bauer, S. E. et al. Global modeling of heterogeneous chemistry on mineral aerosol surfaces: influence on tropospheric ozone chemistry and comparison to observations. *J. Geophys. Res. Atmos.* **109**, <https://doi.org/10.1029/2003JD003868> (2004).
68. Hauglustaine, D. A. & Ehhalt, D. H. A three-dimensional model of molecular hydrogen in the troposphere. *J. Geophys. Res. Atmos.* **107**, <https://doi.org/10.1029/2001JD001156> (2002).

69. Dunne, J. P. et al. The GFDL earth system model version 4.1 (GFDL-ESM 4.1): overall coupled model description and simulation characteristics. *J. Adv. Model. Earth Syst.*, **12**, <https://doi.org/10.1029/2019MS002015> (2020).
70. Horowitz, L. W. et al. The GFDL global atmospheric chemistry-climate model AM4.1: model description and simulation characteristics. *J. Adv. Model. Earth Syst.* **12**, <https://doi.org/10.1029/2019MS002032> (2020).

### Acknowledgements

We would like to thank Jean-François Lamarque for providing the WACCM results and for his valuable input to the study. This study was supported by the HYDROGEN project grants no. 320240 funded by Energix and the Norwegian Research Council. Parts of the simulations were performed on resources provided by Sigma2 - the National Infrastructure for High-Performance Computing and Data Storage in Norway, and the data was also uploaded and shared through their services through the project accounts NN9188K and NS9188K.

### Author contributions

M.S. lead the study and the writing of the paper, R.B.S. ran the OsloCTM model and the GWP calculations, M.S. performed the uncertainty calculations, S.K. ran the UCI CTM model, H.B. ran the UKCA model, D.H. ran the INCA model, and F.P. ran the GFDL model. All the above-mentioned and G.M., R.D., M.P., and D.S. contributed to the design of the study and discussions of the results. All authors contributed to the writing of the paper.

### Competing interests

The authors declare no competing interests.

### Additional information

**Supplementary information** The online version contains supplementary material available at <https://doi.org/10.1038/s43247-023-00857-8>.

**Correspondence** and requests for materials should be addressed to Maria Sand.

**Peer review information** *Communications Earth & Environment* thanks the anonymous reviewers for their contribution to the peer review of this work. Primary Handling Editors: Prabir Patra, Clare Davis, Heike Langenberg. A peer review file is available.

**Reprints and permission information** is available at <http://www.nature.com/reprints>

**Publisher's note** Springer Nature remains neutral with regard to jurisdictional claims in published maps and institutional affiliations.



**Open Access** This article is licensed under a Creative Commons Attribution 4.0 International License, which permits use, sharing, adaptation, distribution and reproduction in any medium or format, as long as you give appropriate credit to the original author(s) and the source, provide a link to the Creative Commons license, and indicate if changes were made. The images or other third party material in this article are included in the article's Creative Commons license, unless indicated otherwise in a credit line to the material. If material is not included in the article's Creative Commons license and your intended use is not permitted by statutory regulation or exceeds the permitted use, you will need to obtain permission directly from the copyright holder. To view a copy of this license, visit <http://creativecommons.org/licenses/by/4.0/>.

© The Author(s) 2023